

Article

Radiative Recombination Studies for Bare Lead Ions Interacting with Low-Energy Electrons

Binghui Zhu ^{1,2,3,*}  and Thomas Stöhlker ^{1,2,3} ¹ Helmholtz Institute Jena, Fröbelstieg 3, 07743 Jena, Germany² GSI Helmholtzzentrum für Schwerionenforschung GmbH, Planckstraße 1, 64291 Darmstadt, Germany³ Institut für Optik und Quantenelektronik, Friedrich-Schiller-Universität Jena, Max-Wien-Platz 1, 07743 Jena, Germany

* Correspondence: b.zhu@hi-jena.gsi.de

Abstract: X-ray emission as a result of radiative recombination (RR) at threshold energies in the electron cooler of CRYRING@ESR was investigated for decelerated bare lead ions at a beam energy of 10 MeV/u. The recorded spectra are dominated by characteristic transitions in Pb⁸¹⁺, namely, the Lyman, Balmer and Paschen series, as a result of decay cascades from high-*n* states that are preferentially populated by the RR processes. In addition, a rigorous theoretical model is applied for the interpretation of measured X-ray spectra, and shows good agreement.

Keywords: X-ray emission; radiative recombination; characteristic transitions; decay cascades



Citation: Zhu, B.; Stöhlker, T. Radiative Recombination Studies for Bare Lead Ions Interacting with Low-Energy Electrons. *Atoms* **2023**, *11*, 2. <https://doi.org/10.3390/atoms11010002>

Academic Editors: Izumi Murakami, Daiji Kato, Hiroyuki A. Sakaue and Hajime Tanuma

Received: 30 September 2022

Revised: 28 November 2022

Accepted: 19 December 2022

Published: 21 December 2022



Copyright: © 2022 by the authors. Licensee MDPI, Basel, Switzerland. This article is an open access article distributed under the terms and conditions of the Creative Commons Attribution (CC BY) license (<https://creativecommons.org/licenses/by/4.0/>).

1. Introduction

Radiative recombination (RR) is the time-reversed process of photoionization and, therefore, one of the most renowned and fundamental processes in atomic physics. In particular, it is also of utmost importance for plasma population dynamics, ionization equilibrium, and radiative power losses. In this process, an electron in continuum state undergoes a direct transition into a bound state of the stationary ion via the emission of a photon carrying away the energy difference between the initial and final electronic state, and satisfying momentum conservation [1].

By studying the X-ray emission produced by electron capture processes into high-*Z* ions, even fine-structure sensitive information can be obtained which provides a stringent test of atomic collision theory [2,3]. With the advent of ion cooler storage rings [4,5] (e.g., the ESR and the CRYRING storage ring at GSI, Darmstadt), one has the possibility to work with a well-known number of ions (10^5 – 10^9) at well-defined speeds and charge states. Further on, the cooling technique adopted makes the ion beam monoenergetic, and reduces the angular divergence and geometrical size of the beam. This gives access to enormous enhancements in X-ray spectroscopy resolution with substantially improved precision [6–8]. In this paper, we will report on and summarize the results of the latest X-ray-emission-related experiment for reliable low-temperature RR studies at the electron cooler of CRYRING@ESR.

2. Experiment

The experimental studies reported in this paper were carried out at the heavy ion cooler storage ring CRYRING@ESR at GSI in Darmstadt [9]. The lead ions were accelerated up to 400 MeV/u in the synchrotron SIS18, then extracted and transferred to the ESR storage ring. Before that, the ions passed through a copper foil with proper thickness, and the desired charged state was selected utilizing bending magnet for *q*/*A* separation. Here, *q* and *A* denote the ionic charge and mass number, respectively. In the electron cooler, the Coulomb interaction between a cold electron beam and a hot ion beam leads to energy and momentum transfer; finally, a thermodynamical equilibrium is reached

resulting in a drastic reduction in the ion beam temperature [10]. After cooling, the ions were decelerated down to a beam energy of close to 10 MeV/u. Eventually, $\sim 10^5$ ions were stored and injected into CRYRING@ESR for further experimental activities. In order to guarantee a well-defined constant beam velocity, generally of the order of $\Delta\beta/\beta \sim 10^{-5}$, electron currents of, typically, 10 to 20 mA were applied at the CRYRING@ESR cooler. Moreover, the electron cooling guarantees a DC ion beam with an approximate diameter of 2 mm and a longitudinal momentum spread of about 10^{-5} .

The layout of the experimental setup at the CRYRING@ESR electron cooler is depicted in Figure 1. Here, the electron cooler also serves as a target of free electrons to study the RR processes. Two dedicated X-ray detection chambers installed behind corresponding dipole magnets [11] allow us to record photon emission from the beam–target interaction volume under 0° and 180° observation angles with respect to the beam direction. In the experiment, two high-purity germanium detectors (Ge(i)) were used, isolated from the ultra-high vacuum of the ring via 100 μm beryllium foils. Each X-ray detector was equipped with an X-ray collimator of a narrow angular acceptance in order to reduce the Doppler broadening. Projectiles capturing one electron from the cooler section were registered by a particle counter behind the first bending magnet downstream from the interaction region.

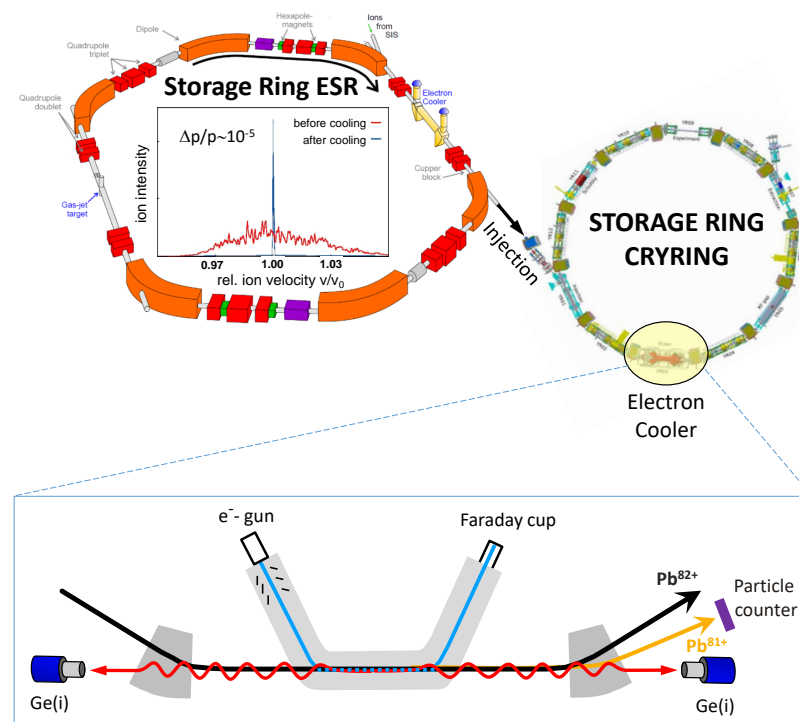


Figure 1. (Top part): Schematic sketch of the coupling of the ESR and the CRYRING storage ring at GSI in Darmstadt. (Bottom part): Experimental setup at the electron cooler of CRYRING@ESR storage ring. The X-ray emission from the electron–ion beam interaction region was viewed by two high-purity Ge(i) detectors under 0° and 180° observation angles with respect to the ion beam direction. X-rays were measured in coincidence with down-charged Pb^{81+} projectiles detected by the particle counter installed behind the electron cooler. Two dedicated vacuum separation chambers, equipped with beryllium view ports, are not shown in the figure.

3. Data Analysis and Results

The interpretation of experimentally recorded X-ray spectra requires an accurate modeling of the RR processes for all relevant levels. The complete levels structure, e.g., transition rates and transition energies, are calculated by the Flexible Atomic Code (FAC) [12], which was proved to be fast and reasonable accurate as compared to the existing reference database [13,14]. For ions interacting with electrons in the electron cooler, the electron beam has a velocity distribution $f(v)$. Therefore, it is more practical to introduce

the so-called RR rate coefficient α_{nlj} instead of the RR cross section σ_{nlj} , which is appropriate for a fixed electron-beam velocity. The rate coefficient α_{nlj} is derived by a convolution of the RR cross section σ_{nlj} with the experimental velocity distribution function $f(v)$ [15],

$$\alpha_{nlj} = \langle v\sigma_{nlj}(\mathbf{v}) \rangle = \int v\sigma_{nlj}(\mathbf{v})f(\mathbf{v})d^3v. \quad (1)$$

The velocity distribution of electrons in the electron cooler is expressed, in the ion projectile frame, as follows [16]

$$f(\mathbf{v}) = \left(\frac{m_e}{2\pi}\right)^{3/2} \frac{1}{kT_{\perp}(kT_{\parallel})^{1/2}} \exp\left[-\left(\frac{m_e v_{\perp}^2}{2kT_{\perp}} + \frac{m_e v_{\parallel}^2}{2kT_{\parallel}}\right)\right]. \quad (2)$$

The beam temperatures T_{\perp} and T_{\parallel} characterize the transverse and longitudinal motion of the electron beam, respectively, and k is the Boltzmann constant. For the calculations of (n, l, j) -dependent RR-rate coefficients distribution, we followed the routine as discussed elsewhere [17,18], in which the numerical evaluation of the RR cross sections in strongly bound states ($n \leq 10$) was performed in a fully relativistic manner following the detailed formulations in Refs. [19,20]. For higher excited states with main quantum numbers $n > 10$, the non-relativistic dipole approximation was applied by making use of a set of recurrence relations introduced by Burgess [21] and finally integrated according to Equation (1). In practice, however, one may expect that, apart from the direct recombination, the feeding transitions from high-lying levels will also contribute to the population of the ionic substates. In this way, states with main quantum number $n = 1$ up to high-Rydberg states such as $n = 165$ were incorporated in the description of subsequent cascade processes [22] by solving a couple of rate equations [23], written as

$$\frac{dN_k(t)}{dt} = -\alpha_k N_k(t) + \sum_{m(>k)} \Gamma_{m \rightarrow k} N_m(t), \quad (3)$$

where α_k is a decay constant (the inverse of the lifetime) for the k state, $N_k(t)$ is the population for the k state at time t and $\Gamma_{m \rightarrow k}$ is a transition rate for the transition from an upper m state to a lower k state.

With input databases of binding energies, transition rates, and initial RR population distributions available, we are able to formulate the X-ray spectroscopy using the radiative cascade function as expressed in Equation (3). Comparisons of the simulated X-ray spectra with the experimental measurements at 0° and 180° observation angles recorded by two Ge(i) detectors are displayed in Figure 2. The experimental spectra registered show RR transitions into the K , L and M shells along with the characteristic Lyman, Balmer and Paschen lines. The random events were already subtracted from the true coincidence X-ray spectrum. For presentation purposes, the theoretical spectra were normalized to the experimental ones by adjusting to the population of the K -RR line. In addition, the spectral line profiles are approximated by a Gaussian function with a FWHM of 550 eV to account for the intrinsic resolution of the X-ray detectors used, whereby contributions from the relative velocities between electrons and ions to the width of the line are negligible. The calculated photon energies were corrected by the Doppler shift, which are dependent on the angles θ between the emitted X-rays and the movement of Pb^{81+} ions, in the mathematical form of

$$E_{lab} = \frac{E_{proj}}{\gamma(1 - \beta \cos\theta)}, \quad (4)$$

where E_{proj} and E_{lab} are, respectively, the X-ray energies in the projectile and in the laboratory frame; β is the beam velocity in unit of speed of light and $\beta = v/c \approx 0.14$ for ion beam energy of 10 MeV/u; and $\gamma = (1 - \beta^2)^{-1/2}$ is the relativistic Lorentz factor.

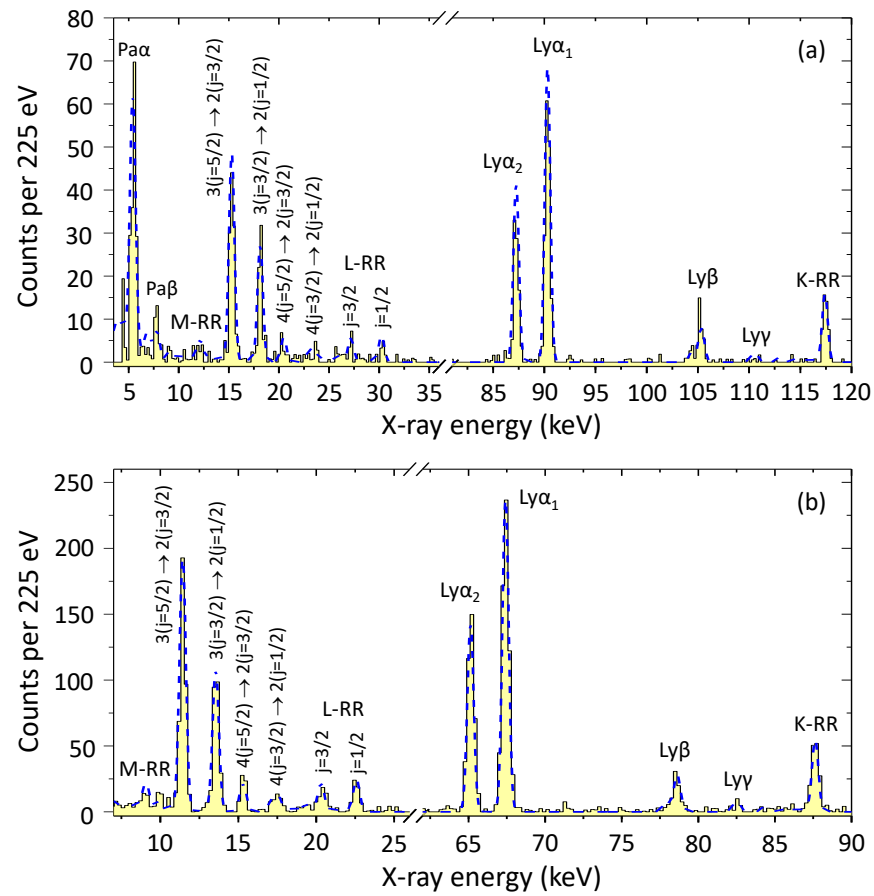


Figure 2. X-ray spectra measured at observation angles of (a) 0° and (b) 180° by two high-purity Ge(i) detectors in coincidence with down-charged Pb^{81+} ions. The blue dashed lines give the result of time-integrated spectra based on a cascade simulation program [22]. Here, the energy dependent efficiencies of two Ge(i) detectors are corrected.

It can be observed that the calculated photon energies by FAC code in combination with Doppler shift corrections show a good agreement with the counterparts of experimental values, and, therefore, serve as a unique probe to identify numerous transition types, as marked in Figure 2. Complementary information on the subshell differentiation for various shells is provided by the population pattern of radiative transitions. Since the photon intensities in the direct RR processes are proportional to the recombination rate coefficients, the corresponding X-ray spectrum for the prompt *L*-RR and *M*-RR processes can be obtained straightforwardly from the relative values of state-selective recombination rate coefficients. These relative values of rate coefficients also constitute the initial populations in the sequential cascade processes, in which the X-ray spectrum from radiative decay cascades can be calculated by the branching ratios decaying into different final states. Based on the comparison with the observed (relative) Lyman- α line intensities, we conclude that there is a really significant contribution of above 90% to the Lyman- α emission arising from recombination into high Rydberg states and subsequent cascades. Most remarkably, photon energies below 20 keV in the range of Balmer and Paschen transitions, which were blocked by stainless-steel windows at the ESR [24,25], were observed for the first time due to the two beryllium window chambers installed behind the two dipole magnets. In the case of the Balmer series, a multitude of transitions, basically due to the fine-structure splitting of the $n = 2$ and $n = 3$ states, are clearly visible in both X-ray detectors. Following the radiative cascade simulation procedure [22], the most populated states $3d_{5/2}$ and $3d_{3/2}$ resulting from Yrast-Cascades chain contribute to the formation of two intense Balmer lines, which are the transitions of $3d_{5/2} \rightarrow 2p_{3/2}$ (Balmer- α_1) and $3d_{3/2} \rightarrow 2p_{1/2}$ (Balmer- α_2), as observed in this experiment shown in Figure 2. Only small discrepancies are observed in the region of

Paschen lines. These are most likely the result of a low-energy asymmetry of peak profiles that arise from the missing resolution of the X-ray detector, and are partially due to the spectrum absorption effects in the beryllium window that are not regarded thoroughly at the low-energy part. Within the statistical accuracy, the time-integrated line intensity ratios for both X-ray detectors appear to be in excellent agreement with the results from cascade calculations, as depicted in Figure 3. It is worth mentioning that the $L\text{-RR}_{j=3/2}/L\text{-RR}_{j=1/2}$ representing the intensity ratio of $\text{Ly-}\alpha_1/\text{Ly-}\alpha_2$ at $t = 0$ (prompt X-ray emission) does not follow the rule of statistical weights considered in nonrelativistic treatment [26]. In general, it appears that the relative intensity ratios are well-reproduced for both observation angles, which indicates that the theoretical calculations are qualitatively in harmony with the measured spectra and seems to prove our radiative cascade simulation program can be an important tool for studying recombination processes.

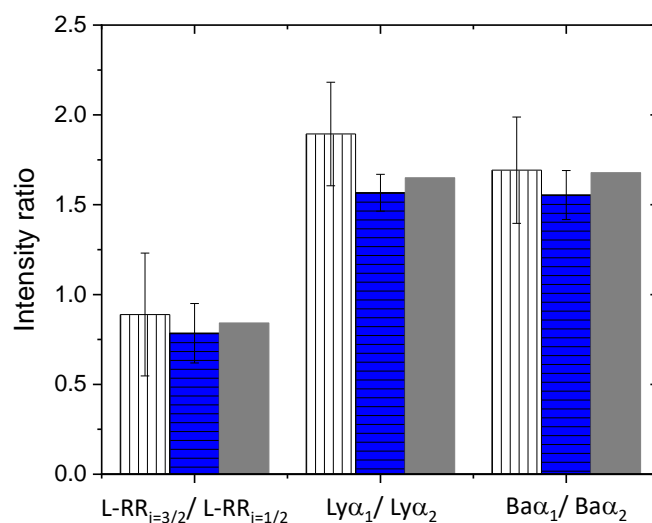


Figure 3. Experimental results of the line intensity ratios in comparison with the time-dependent theoretical model (gray columns) for fine-structure resolved L -RR radiations and characteristic X-ray lines. White columns with vertical strips show experimental data at 0° , blue columns with horizontal strips show experimental data at 180° .

4. Conclusions

In the first dedicated beam time at the CRYRING@ESR, state-selective information of the substructure in excited states via the RR of initially bare lead ions with low-energy free electrons were obtained. The feasibility of the experimental method and the rigorous cascade simulation program is confirmed for studying a one-electron system in hydrogen-like high- Z ions. An experimental investigation of the radiative decay modes from high Rydberg states to the formation of sequential Balmer series and $L \rightarrow K$ transitions in Pb^{81+} ions was presented.

In the near future, one may aim at the measurement of absolute X-ray line intensities, in contrast to intensity ratios as applied in the present study. Such studies conducted at the electron cooler of CRYRING@ESR may dramatically enhance the sensitivity to higher Rydberg states and be used to explore the origin of the so-called rate enhancement observed, up to now, only for total RR rates [27].

Author Contributions: Writing—original draft, B.Z.; Writing—review and editing, B.Z.; Supervision, T.S. All authors have read and agreed to the published version of the manuscript.

Funding: This research was conducted in the framework of the SPARC collaboration, experiment E138 of FAIR Phase-0 supported by GSI. It is further supported by the Extreme Matter Institute EMMI and by the European Research Council (ERC) under the European Union’s Horizon 2020 research.

Data Availability Statement: Not applicable.

Acknowledgments: B.Z. acknowledges the financial support from Chinese Scholarship Council (Grant No. 201806180051) and Helmholtz Institute Jena for his stay in Germany finalizing the doctoral project.

Conflicts of Interest: The authors declare no conflict of interest.

References

1. Hahn, Y. Electron-ion recombination processes—An overview. *Rep. Prog. Phys.* **1997**, *60*, 691–759. [CrossRef]
2. Eichler, J. *Lectures on Ion-Atom Collisions: From Nonrelativistic to Relativistic Velocities*, 1st ed.; ELSEVIER: Amsterdam, The Netherlands, 2005; pp. 81–193.
3. Eichler, J.; Stöhlker, T. Radiative electron capture in relativistic ion–atom collisions and the photoelectric effect in hydrogen-like high-Z systems. *Phys. Rep.* **2007**, *439*, 1–99. [CrossRef]
4. Schuch, R. Storage rings for low-energy experiments. *Phys. Scr.* **1995**, *T59*, 77–86. [CrossRef]
5. Durante, M.; Indelicato, P.; Jonson, B.; Koch, V.; Langanke, K.; Meißner, U.-G.; Nappi, E.; Nilsson, T.; Stöhlker, T.; Widmann, E.; et al. All the fun of the FAIR: Fundamental physics at the facility for antiproton and ion research. *Phys. Scr.* **2019**, *94*, 033001. [CrossRef]
6. Gumberidze, A.; Stöhlker, T.; Banaś, D.; Beckert, K.; Beller, P.; Beyer, H.F.; Bosch, F.; Cai, X.; Hagmann, S.; Kozhuharov, C.; et al. Electron-electron interaction in strong electromagnetic fields: The two-electron contribution to the ground-state energy in He-like uranium. *Phys. Rev. Lett.* **2004**, *92*, 203004. [CrossRef]
7. Gumberidze, A.; Stöhlker, T.; Banaś, D.; Beckert, K.; Beller, P.; Beyer, H.F.; Bosch, F.; Hagmann, S.; Kozhuharov, C.; Liesen, D.; et al. Quantum electrodynamics in strong electric fields: The ground-state Lamb shift in hydrogenlike uranium. *Phys. Rev. Lett.* **2005**, *94*, 223001. [CrossRef]
8. Banaś, D.; Pajek, M.; Surzhykov, A.; Stöhlker, T.; Brandau, C.; Gumberidze, A.; Kozhuharov, C.; Beyer, H.F.; Böhm, S.; Bosch, F.; et al. Subshell-selective X-ray studies of radiative recombination of U^{92+} ions with electrons for very low relative energies. *Phys. Rev. A* **2015**, *92*, 032710. [CrossRef]
9. Lestinsky, M.; Andrianov, V.; Aurand, B.; Bagnoud, V.; Bernhardt, D.; Beyer, H.; Bishop, S.; Blaum, K.; Bleile, A.; Borovik, A., Jr.; et al. Physics book: CRYRING@ESR. *Eur. Phys. J. Spec. Top.* **2016**, *225*, 797–882. [CrossRef]
10. Poth, H. Electron cooling: Theory, experiment, application. *Phys. Rep.* **1990**, *196*, 135–297. [CrossRef]
11. Pfäfflein, P.; Allgeier, S.; Bernitt, S.; Fleischmann, A.; Friedrich, M.; Hahn, C.; Hengstler, D.; Herdrich, M.O.; Kalinin, A.; Kröger, F.M.; et al. Integration of maXs-type microcalorimeter detectors for high-resolution X-ray spectroscopy into the experimental environment at the CRYRING@ESR electron cooler. *Phys. Scr.* **2022**, *97*, 114005. [CrossRef]
12. Gu, M.F. The flexible atomic code. *Can. J. Phys.* **2008**, *86*, 675–689. [CrossRef]
13. Pal'chikov, V.G. Relativistic transition probabilities and oscillator strengths in hydrogen-like atoms. *Phys. Scr.* **1998**, *57*, 581–593. [CrossRef]
14. Yerokhin, V.A.; Shabaev, V.M. Lamb shift of $n = 1$ and $n = 2$ states of hydrogen-like atoms, $1 \leq Z \leq 110$. *J. Phys. Chem. Ref. Data* **2015**, *44*, 033103. [CrossRef]
15. Pajek, M.; Schuch, R. Radiative recombination of bare ions with low-energy free electrons. *Phys. Rev. A* **1992**, *45*, 7894–7905. [CrossRef]
16. Danared, H.; Andler, G.; Bagge, L.; Herrlander, C.J.; Hilke, J.; Jeansson, J.; Källberg, A.; Nilsson, A.; Paál, A.; Rensfelt, K.-G.; et al. Electron cooling with an ultracold electron beam. *Phys. Rev. Lett.* **1994**, *72*, 3775–3778. [CrossRef]
17. Brinzaescu, O.; Eichler, J.; Ichihara, A.; Shirai, T.; Stöhlker, T. Comparison between the nonrelativistic dipole approximation and the exact relativistic theory for radiative recombination. *Phys. Scr.* **1999**, *T80*, 324–325. [CrossRef]
18. Brinzaescu, O.; Stöhlker, T. Radiative recombination rate coefficients. *Phys. Scr.* **2001**, *T92*, 275–277. [CrossRef]
19. Pratt, R.H.; Ron, A.; Tseng, H.K. Atomic photoelectric effect above 10 keV. *Rev. Mod. Phys.* **1973**, *45*, 273–325. [CrossRef]
20. Ichihara, A.; Eichler, J. Cross sections for radiative recombination and the photoelectric effect in the K, L, and M shells of one-electron systems with $1 \leq Z \leq 112$ calculated within an exact relativistic description. *At. Data Nucl. Data Tables* **2000**, *74*, 1–121. [CrossRef]
21. Burgess, A. Tables of hydrogenic photoionization cross-sections and recombination coefficients. *Mem. R. Astron. Soc.* **1965**, *69*, 1. Available online: <https://ui.adsabs.harvard.edu/abs/1965MmRAS..69....1B/abstract> (accessed on 29 September 2022).
22. Zhu, B.; Gumberidze, A.; Over, T.; Weber, G.; Andelkovic, Z.; Bräuning-Demian, A.; Chen, R.J.; Dmytriev, D.; Forstner, O.; Hahn, C.; et al. X-ray emission associated with radiative recombination for Pb^{82+} ions at threshold energies. *Phys. Rev. A* **2022**, *105*, 052804. [CrossRef]
23. Curtis, L.J. A Diagrammatic mnemonic for calculation of cascading level populations. *Am. J. Phys.* **1968**, *36*, 1123–1125. [CrossRef]
24. Gumberidze, A.; Stöhlker, T.; Bednarz, G.; Beyer, H.F.; Bosch, F.; Cai, X.; Hagmann, S.; Klepper, O.; Kozhuharov, C.; Liesen, D.; et al. X-ray transitions studied for decelerated bare and H-like uranium ions at the ESR electron cooler. *Nucl. Instrum. Methods Phys. Res. Sect. B* **2003**, *205*, 374–377. [CrossRef]
25. Reuschl, R.; Gumberidze, A.; Stöhlker, T.; Kozhuharov, C.; Rządkiwicz, J.; Spillmann, U.; Tashenov, S.; Fritzsche, S.; Surzhykov, A. The Balmer spectrum of H-like uranium produced by radiative recombination at low velocities. *Radiat. Phys. Chem.* **2006**, *75*, 1740–1743. [CrossRef]

26. Reuschl, R.; Gumberidze, A.; Kozhuharov, C.; Spillmann, U.; Tashenov, S.; Stöhlker, T.; Eichler, J. State-selective X-ray studies of radiative recombination into bare and H-like uranium at threshold energies. *Phys. Rev. A* **2008**, *77*, 032701. [[CrossRef](#)]
27. Shi, W.; Böhm, S.; Böhme, C.; Brandau, C.; Hoffknecht, A.; Kieslich, S.; Schippers, S.; Müller, A.; Kozhuharov, C.; Bosch, F. Recombination of U^{92+} ions with electrons. *Eur. Phys. J. D* **2001**, *15*, 145–154. [[CrossRef](#)]

Disclaimer/Publisher's Note: The statements, opinions and data contained in all publications are solely those of the individual author(s) and contributor(s) and not of MDPI and/or the editor(s). MDPI and/or the editor(s) disclaim responsibility for any injury to people or property resulting from any ideas, methods, instructions or products referred to in the content.